

promoting access to White Rose research papers



Universities of Leeds, Sheffield and York
<http://eprints.whiterose.ac.uk/>

This is the publisher's version of a Proceedings Paper presented at the **2010 IEEE International Ultrasonics Symposium**

Harput, S, Arif, M and Freear, S (2010) *Experimental investigation of the subharmonic emission from microbubbles using linear and nonlinear frequency modulated signals*. In: Proceedings - IEEE Ultrasonics Symposium. UNSPECIFIED. IEEE , 1724 - 1727. ISBN 978-1-4577-0382-9

White Rose Research Online URL for this paper:

<http://eprints.whiterose.ac.uk/id/eprint/75991>

Experimental Investigation of the Subharmonic Emission from Microbubbles using Linear and Nonlinear Frequency Modulated Signals

Sevan Harput, Muhammad Arif and Steven Freear
Ultrasound Group, School of Electronic and Electrical Engineering, University of Leeds.

Abstract—In medical ultrasound imaging, coded excitation is widely used to increase signal to noise ratio (SNR) and penetration without increasing the peak pressure level by using longer pulse durations. The aim of this work is to utilize chirp coded excitation and investigate the effect on subharmonic emission from contrast agents for nondestructive subharmonic imaging. The subharmonic emission of the microbubbles is measured as a function of pressure and bandwidth for linear frequency modulated (LFM) and nonlinear frequency modulated (NLFM) signals. Results indicate that for both excitation schemes, narrow-band signals produced higher subharmonic level. It is also observed that for wide-band signals, NLFM excitation generated the highest subharmonic level.

I. INTRODUCTION

The nonlinear behavior of ultrasound contrast agents (UCAs) has attracted a great attention in medical ultrasound imaging [1]. UCAs mostly scatter the acoustic energy at the fundamental frequency, but also generate second harmonic, subharmonic and ultra-harmonic frequencies even at low pressure levels. These nonlinear harmonic components generated by microbubbles are used in ultrasound contrast imaging to improve the contrast and allow a selective detection during perfusion [2].

Nowadays, second harmonic imaging is available in commercial ultrasound imaging systems. Second harmonic imaging improves the axial resolution, but human tissue can also generate the second harmonic, which degrades the contrast-to-tissue ratio (CTR) [3]. However, subharmonic energy at low acoustic pressures is only generated by microbubble contrast agents [4]. The lower frequency of the subharmonic component causes a reduction in axial resolution, but improves the penetration depth due to less attenuation [5].

It has been already demonstrated that subharmonic generation is highly related with the excitation waveform and frequency [6]. Microbubbles can efficiently generate subharmonic components at low acoustic pressures when the excitation frequency is twice the resonance frequency of the microbubbles [7]. However, the effect of the waveform on subharmonic generation is still not clear and needs to be studied. The aim of this work is to investigate the effect of chirp coded excitation for nondestructive subharmonic imaging. The subharmonic generation of microbubbles is measured by using sinusoidal tone-burst, LFM and NLFM excitation with 10%, 20%, and 40% fractional bandwidths at peak negative pressures below 200 kPa.

II. CODED EXCITATION

Coded excitation techniques have been applied to medical ultrasound systems to improve the image quality. These coding techniques provide improved SNR and increase the penetration depth without increasing the peak acoustic pressure. The chirp coded signals or frequency modulated signals are designed to have long duration and wide bandwidth compared to conventional sinusoidal tone-burst excitation techniques. The transmission of a long duration chirp signal increases the total energy, which increases the SNR and penetration depth. However, increasing the signal duration does not reduce the axial resolution. On the receiving side, the chirp signals are compressed using a matched filter. After pulse compression, the axial resolution of the compressed chirp signal is comparable to a pulse with same bandwidth [8].

A. Frequency Modulated Signals

A frequency modulated signal, $s(t)$, can be expressed as,

$$s(t) = p(t) e^{j2\pi \int f_i(t) dt}, \quad 0 \leq t \leq T$$

where $p(t)$ is the amplitude modulation function and $f_i(t)$ is the instantaneous frequency of the signal.

The instantaneous frequency, $f_i(t)$, of a LFM signal can be expressed as,

$$f_i(t) = \frac{B}{T}t + \left(f_c - \frac{B}{2}\right)$$

where B is the sweeping bandwidth, T is the time duration, and f_c is the center frequency of the chirp signal.

The spectrum of the NLFM signal is matched with the transfer function of the ultrasound measurement system. This allows the NLFM signal to provide more SNR improvement than the LFM signal. The NLFM signal can be designed by using the nonlinear instantaneous frequency function, $f_i(t)$, containing the LFM and tangent FM functions as [9],

$$f_i(t) = f_c + \frac{B}{2} \left[\frac{\alpha \tan\left(\frac{2\gamma t}{T}\right)}{\tan(\gamma)} + \frac{2(1-\alpha)t}{T} \right]$$

where parameters α and γ are adjusted to control the nonlinear FM curve. In this work, the NLFM signals are designed with $\alpha = 0.4$ and $\gamma = 1.2$.

For both chirps, phase of the complex signal $s(t)$ can be obtained by computing the integral of the instantaneous frequency function.

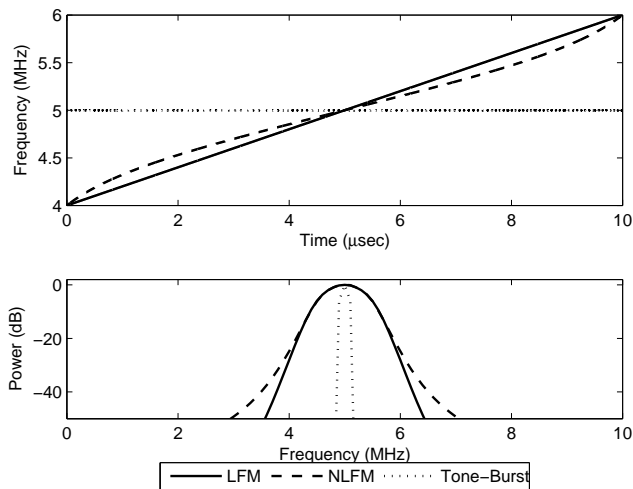


Fig. 1. The figure shows the instantaneous frequency (top) and power spectra (bottom) of the LFM (solid line), NLFM (dash line), and tone-burst (dotted line) excitation signals.

III. MATERIALS AND METHODS

A. Excitation Signals

In all simulations and experiments, LFM, NLFM and tone-burst signals are used for excitation. For LFM and NLFM signals, 10%, 20% and 40% fractional bandwidths are used. The NLFM signal parameters α and γ are chosen to obtain a power spectrum which contain less ripples and has a -3 dB bandwidth similar to the LFM signal. A special window is designed for the NLFM signal as explained by Collins and Atkins [9], however a Hann window is applied to the tone-burst and LFM signals in order to reduce spectral ripples.

Instantaneous frequencies and power spectra of the excitation signals are shown in Figure 1. Only LFM and NLFM signals with 40% fractional bandwidth are shown in this figure.

B. Simulations

Recently, it is observed that the *compression-only* behavior of the microbubbles is responsible for subharmonic generation [10]. The Rayleigh-Plesset equation is successfully modified by Marmottant *et al.* to model the compression-only behavior of the coated microbubbles at low acoustic pressures [11]. The model realistically describes the behavior of phospholipid coated microbubbles by defining the surface tension as a function of microbubble radius. The equation of radial motion of phospholipid coating microbubble including the effective surface tension is expressed by [11],

$$\rho \left(R\ddot{R} + \frac{3}{2}\dot{R}^2 \right) = \left(P_0 + \frac{2\sigma_w}{R_0} \right) \left(\frac{R}{R_0} \right)^{-3\kappa} \left(1 - \frac{3\kappa}{c}\dot{R} \right) - \frac{2\sigma(R)}{R} - \frac{4\mu\dot{R}}{R} - \frac{4\kappa_S\dot{R}}{R^2} - P_0 - P_{ac}(t)$$

where R is the instantaneous bubble radius, \dot{R} is the velocity of the bubble wall, \ddot{R} is the acceleration of the bubble wall, and R_0 is the radius of the bubble at equilibrium, P_0 is the

ambient pressure, $P_{ac}(t)$ is the acoustic driving pressure, ρ is the density of the water, c is the speed of sound in the water, κ is polytropic gas exponent, σ_w is the surface tension of water, μ is the viscosity of the liquid and κ_S is the shell viscosity.

The effective surface tension $\sigma(R)$ of phospholipid coated microbubble have three states; buckling, elastic, ruptured. In the buckling state $\sigma(R) = 0$, where the shell loses its surface tension because the bubble is compressed too much. In the elastic state the surface tension can be calculated as $\sigma(R) = \chi(R^2/R_{buckling}^2 - 1)$, where χ is the shell elasticity. The shell molecules are separated in the rupture state due to expansion and the surface tension becomes the same as water, $\sigma(R) = \sigma_w$. The buckling and rupture radii are defined as

$$R_{buckling} = R_0 \text{ and } R_{rupture} = R_{buckling} \sqrt{1 + \sigma_w/\chi}.$$

The pressure radiated by the microbubble is calculated as [12],

$$P_s = \rho \frac{R}{d} (2\dot{R}^2 + R\ddot{R})$$

where $d = 10 \text{ mm}$ is taken as a distance from the microbubble.

The SonoVue[®] contrast agent (Bracco Research SA, Milan, Italy), which have a phospholipid shell and a sulfur hexafluoride (SF₆) gas core, was used in the experiments. Thus, the simulation parameters are chosen according to the properties of SonoVue microbubbles; $\kappa = 1.095$ for SF₆, $\kappa_S = 4 \times 10^{-9} \text{ kg/s}$ and $\chi = 0.3 \text{ N/m}$ for the phospholipid shell [13]. The bubble radius at equilibrium, R_0 , is chosen as $1.7 \mu\text{m}$, since the average bubble radius drops down to below $2 \mu\text{m}$ after few minutes of decantation [14].

C. Experiments

The scattering properties of SonoVue contrast agent were measured using sinusoidal tone-burst, LFM and NLFM excitations. A cylindrical chamber containing the 1:1000 diluted SonoVue suspension was immersed in de-gassed water at 20°C and mixed with a magnetic stirrer during the experiments. The chamber had two acoustically transparent windows, one for transmitting and the other for receiving the scattered acoustic waves. It is known that the average resonance frequency for the native population of SonoVue microbubbles is less than 2 MHz. However, after a few minutes of decantation the mean microbubble size dramatically decreases, so an excitation frequency of 5 MHz is chosen to excite the microbubbles at twice of their resonance frequency. A 5 MHz V310 transducer (Olympus-NDT Inc., Waltham, MA, USA) mounted perpendicular to a 1 mm needle hydrophone (Precision Acoustics Ltd., Dorchester, UK) was placed 10 mm from the chamber. Microbubbles were acoustically excited for 10 μs with peak negative pressures up to 200 kPa.

Excitation signals were designed in Matlab (Mathworks Inc., Natick, MA, USA) and then loaded into 33250A arbitrary waveform generator (Agilent Technologies Inc., Santa Clara, CA, USA). The generated signals were amplified with a E&I A150 RF power amplifier (Electronics & Innovation Ltd., Rochester, NY, USA) and then used to drive the 5 MHz transducer.

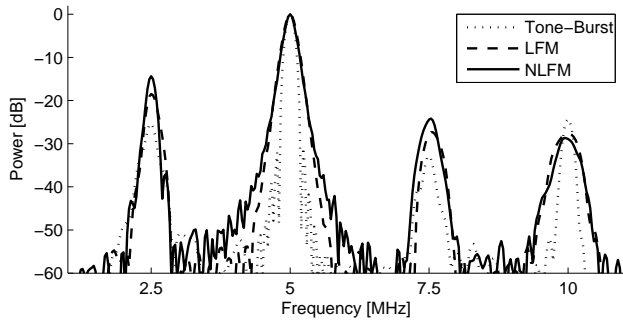


Fig. 2. Simulation results showing power spectra of the scattered signals from 1.7 μm radius coated microbubble at 50 kPa.

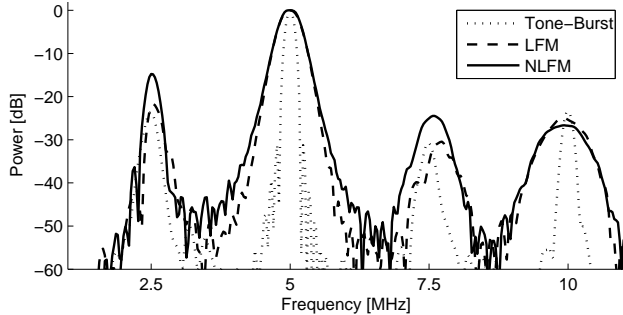


Fig. 3. Simulation results showing power spectra of the scattered signals from 1.7 μm radius coated microbubble at 100 kPa.

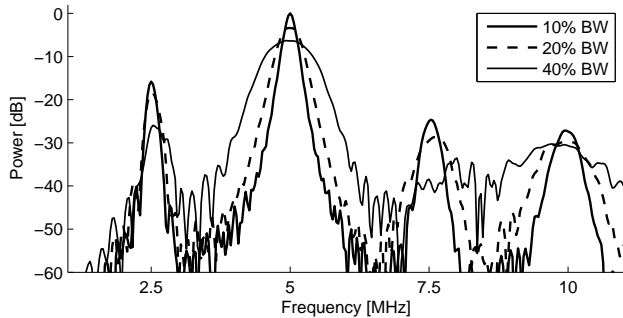


Fig. 4. Simulation results showing power spectra of the scattered signals from 1.7 μm radius coated microbubble for NLFM excitation of 10%, 20% and 40% bandwidth at 100 kPa.

For each excitation method, 64 measurements were taken at each pressure and the average scattered power calculated in the frequency domain. The received signals were first amplified by 59 dB with 5072-PR pulser/receiver (Panametrics-NTD, Inc., Waltham, MA, USA) and then digitized by a LeCroy 64xi digital oscilloscope (LeCroy Corporation, Chestnut Ridge, NY, USA). The captured data from the oscilloscope was transferred to a personal computer and processed in Matlab.

IV. RESULTS AND DISCUSSION

A. Simulations

Figure 2 shows power spectra of the scattered signals from 1.7 μm radius coated microbubble for LFM, NLFM and tone-burst excitations with 10% fractional bandwidth at 50 kPa. The subharmonic component for NLFM excitation is 15 dB

TABLE I
SUBHARMONIC POWER IN DECIBELS

	Tone-Burst		LFM		NLFM		
	10%	20%	40%	10%	20%	40%	
25 kPa	-	0.2	1.0	-	-	-	-
50 kPa	1.6	14.8	2.5	1.4	5.8	7.4	2.2
100 kPa	8.2	22.3	9.6	8.8	19.3	18.5	12.8
150 kPa	15.0	24.7	17.6	15.9	23.9	23.6	19.6
200 kPa	20.3	25.2	21.2	19.6	27.2	24.4	22.6

below the fundamental component and it is 4 dB and 10 dB higher than the LFM and tone-burst excitations respectively. Similarly, in Figure 3 NLFM excitation has higher subharmonic level with 20% fractional bandwidth at 100 kPa. The subharmonic component for NLFM excitation is 15 dB below the fundamental component and it is 7 dB and 9 dB higher than the LFM and tone-burst excitations respectively. For the same excitation pressure and duration, the subharmonic response for NLFM excitation is always higher than the LFM and tone-burst excitations.

Figure 4 shows power spectra of the scattered signals from 1.7 μm radius coated microbubble for NLFM excitation of 10%, 20% and 40% bandwidth at 100 kPa. It is shown that increasing the excitation bandwidth will cause reduction of the subharmonic response. The subharmonic power of the NLFM excitation with 10% bandwidth is 2.5 dB higher than the 20% bandwidth excitation and 10 dB higher than the 40% bandwidth excitation.

B. Experiments

The scattered subharmonic power is measured for all excitation signals at different pressure levels. The values are normalized according to the noise level and listed in Table I. Unlike the simulations, at 25 kPa the subharmonic component is not clearly observed for all excitations since this pressure level is as low as the subharmonic generation threshold. It is observed that the power level of subharmonic component is decreased with increasing signal bandwidth as expected by the simulations. The power level of subharmonic component for narrow bandwidth (10%) excitation is higher than the wide bandwidth (40%) excitation. NLFM excitation with 10% bandwidth generates 6.5 dB, 4.3 dB and 4.6 dB higher subharmonic levels than NLFM excitation with 40% bandwidth at 100 kPa, 150 kPa and 200 kPa, respectively. It is also found that for wide-band excitation the NLFM signal gives higher subharmonic levels than the LFM signal.

Figures 5 shows power spectra of the scattered signals for LFM and NLFM excitations with 10% fractional bandwidth at 50 kPa. In the simulations, for all cases NLFM excitation had higher subharmonic level than the other excitations. However in the experiments, LFM had higher subharmonic level than the NLFM for 10% fractional bandwidth. For 20% and 40% bandwidths, NLFM excitation gives the highest subharmonic level at every pressure level. Figures 6 shows power spectra

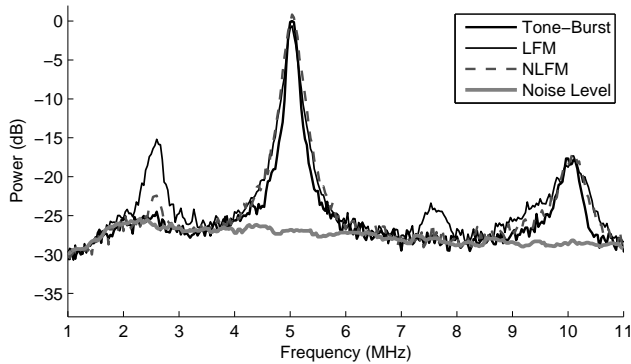


Fig. 5. Power spectra of the scattered signals from SonoVue microbubbles for tone-burst, LFM (10% BW) and NLFM (10% BW) excitations at 50 kPa.

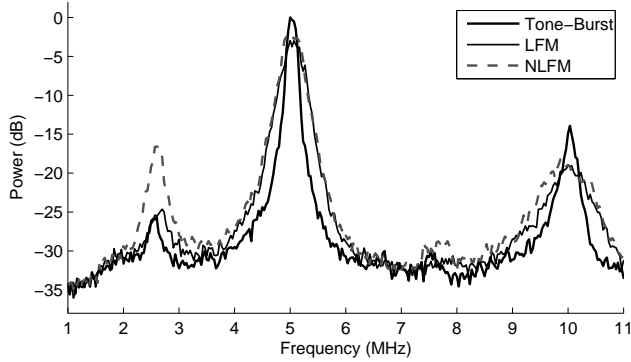


Fig. 6. Power spectra of the scattered signals from SonoVue microbubbles for tone-burst, LFM (20% BW) and NLFM (20% BW) excitations at 100 kPa.

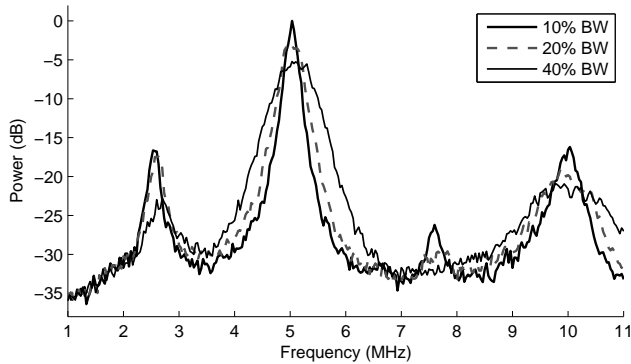


Fig. 7. Power spectra of the scattered signals from SonoVue microbubbles for NLFM excitation of 10%, 20% and 40% bandwidth at 100 kPa.

of the scattered signals for LFM and NLFM excitations with 20% fractional bandwidth at 100 kPa, where the results match with the simulations.

Figures 7 shows power spectra of the scattered signals for NLFM excitation of 10%, 20% and 40% fractional bandwidths at 100 kPa. The experimental measurements completely matches with subharmonic power levels predicted from the simulations. Marmottant's model successfully predicts the subharmonic behavior at low pressures, however above 100 kPa the simulation results and experimental measurements do not match with each other.

V. CONCLUSION

Subharmonic response from contrast microbubbles was measured using linear and nonlinear frequency modulated signals and the results were compared with conventional tone-burst signals. Simulation and experimental results show similar values at low pressure levels below 100 kPa. In simulations the subharmonic level stops rising for the pressures above 100 kPa, however in the experiments it is observed that the subharmonic generation increases with the increasing pressure.

Both in the experiments and simulations, it is observed that LFM and NLFM excitations provide better subharmonic generation than the tone-burst excitation. The results also indicate that the increase of the excitation bandwidth will reduce the power of nonlinear subharmonic component. A wide bandwidth (40%) signal excitation provides lower subharmonic power than the narrow bandwidth (10%) excitation. However, the subharmonic component for the wide bandwidth (40%) excitation will provide better axial resolution after pulse compression. For this reason, NLFM excitation will give the best result for subharmonic imaging since the subharmonic emission was higher for the NLFM excitation.

REFERENCES

- [1] N. de Jong, P. J. A. Frinking, A. Bouakaz, and F. J. T. Cate, "Detection procedures of ultrasound contrast agents," *Ultrasonics*, vol. 38, no. 1-8, pp. 87 – 92, 2000.
- [2] N. de Jong, M. Emmer, A. van Wamel, and M. Versluis, "Ultrasonic characterization of ultrasound contrast agents," *Medical and Biological Engineering and Computing*, vol. 47, no. 8, pp. 861–873, 2009.
- [3] F. A. Duck, "Nonlinear acoustics in diagnostic ultrasound," *Ultrasound in Medicine & Biology*, vol. 28, no. 1, pp. 1–18, 2002.
- [4] P. D. Krishna, P. M. Shankar, and V. L. Newhouse, "Subharmonic generation from ultrasonic contrast agents," *Physics in Medicine and Biology*, vol. 44, no. 3, pp. 681–694, 1999.
- [5] F. Forsberg, W. T. Shi, and B. B. Goldberg, "Subharmonic imaging of contrast agents," *Ultrasonics*, vol. 38, no. 1-8, pp. 93–98, 2000.
- [6] E. Biagi, L. Breschi, E. Vannacci, and L. Masotti, "Subharmonic emissions from microbubbles: effect of the driving pulse shape," *Ultrasonics, Ferroelectrics and Frequency Control, IEEE Transactions on*, vol. 53, no. 11, pp. 2174–2182, 2006.
- [7] A. Eller and H. G. Flynn, "Generation of subharmonics of order one-half by bubbles in a sound field," *The Journal of the Acoustical Society of America*, vol. 46, no. 3B, pp. 722–727, 1969.
- [8] T. Misaridis and J. Jensen, "Use of modulated excitation signals in medical ultrasound. part i: basic concepts and expected benefits," *Ultrasonics, Ferroelectrics and Frequency Control, IEEE Transactions on*, vol. 52, no. 2, pp. 177–191, 2005.
- [9] T. Collins and P. Atkins, "Nonlinear frequency modulation chirps for active sonar," in *Radar, Sonar and Navigation, IEE Proceedings*, vol. 146, no. 6, 1999, pp. 312–316.
- [10] N. de Jong, M. Emmer, C. T. Chin, A. Bouakaz, F. Mastik, D. Lohse, and M. Versluis, "Compression-only behavior of phospholipid-coated contrast bubbles," *Ultrasound in Medicine & Biology*, vol. 33, no. 4, pp. 653–656, 2007.
- [11] P. Marmottant, S. van der Meer, M. Emmer, M. Versluis, N. de Jong, S. Hilgenfeldt, and D. Lohse, "A model for large amplitude oscillations of coated bubbles accounting for buckling and rupture," *The Journal of the Acoustical Society of America*, vol. 118, no. 6, pp. 3499–3505, 2005.
- [12] S. Hilgenfeldt, D. Lohse, and M. Zomack, "Response of bubbles to diagnostic ultrasound: a unifying theoretical approach," *The European Physical Journal B*, vol. 4, no. 2, pp. 247–255, 1998.
- [13] J. Tu, J. Guan, Y. Qiu, and T. J. Matula, "Estimating the shell parameters of sonovue microbubbles using light scattering," *The Journal of the Acoustical Society of America*, vol. 126, no. 6, pp. 2954–2962, 2009.
- [14] J.-M. Gorce, M. Arditi, and M. Schneider, "Influence of bubble size distribution on the echogenicity of ultrasound contrast agents: A study of sonovue," *Investigative Radiology*, vol. 35, no. 11, pp. 661–671, 2000.